

PE&RS

October 2012

Volume 78, Number 10

Oil Thickness

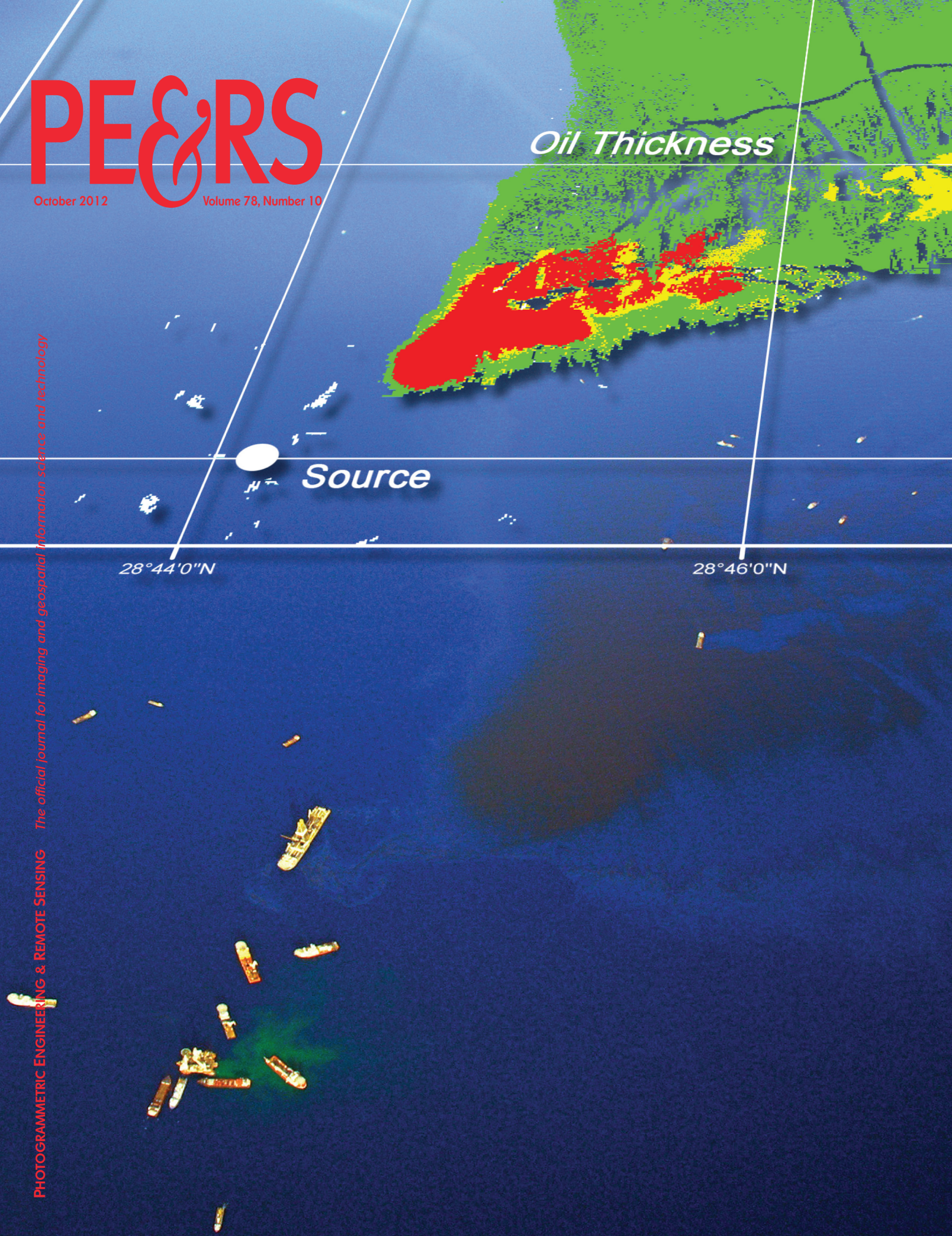
Source

28°44'0"N

28°46'0"N

PHOTOGRAMMETRIC ENGINEERING & REMOTE SENSING The official journal for imaging and geospatial information science and technology

PHOTOGRAMMETRIC ENGINEERING & REMOTE SENSING



This image composite shows an aerial photo of the region around

the source site of the Deepwater Horizon (MC-252) oil spill in the Gulf of Mexico on 5/26/2010. Overlaid is an oil thickness distribution map derived from Ocean Imaging Corp.'s aerial multi-spectral mapping system. The system's oil thickness derivation algorithm used three channels in the visible, one in the near-IR and one in the thermal-IR to assign the oil-containing pixels into several thickness classes. Such GIS-compatible maps of the source region and other regions of priority within the spill were generated once to twice daily and electronically disseminated to the response community. More details on the imaging and how it was utilized throughout the response can be found in a peer-reviewed article in this issue. The surface oil signature is displaced from the actual bottom source location due to currents that affected the oil as it took 4+ hours to rise from the 1500m depth. The greenish feature between the vessels in the lower left corresponds to residual drilling mud used during one of several different attempts to inject material into and plug the leaking well. For more information on the system and Ocean Imaging Corp. see www.oceani.com or call 858-792-8529. Cover image art by Paula Klein, Ocean Imaging.



Highlight Article

1011 Expanding the Utility of Remote Sensing Data for Oil Spill Response

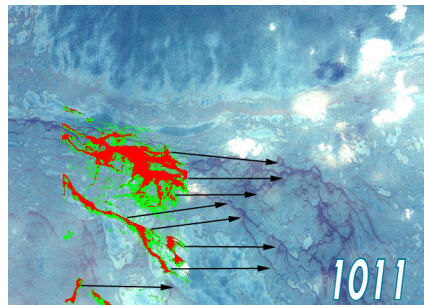
Jan Svejtkovsky and Mark Hess

Columns & Updates

1015 Grids and Datums – Maps in the Middle of Nowhere

1017 Book Review – *Remote Sensing and Global Environmental Change, First Edition*

1020 Industry News

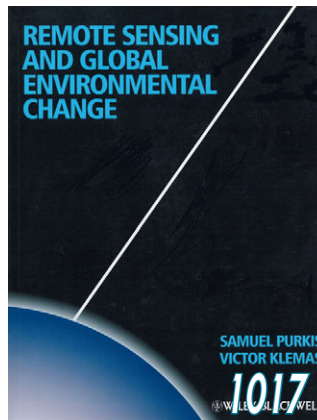


Announcements

1005 New from ASPRS – *Manual of Airborne Topographic Lidar*

1023 ASPRS 2013 Annual Conference – *Confluence by the Bay – A Gathering of Geospatial Insights*

1068 Call for Papers – *Geospatial Responses to Disasters: A Holistic Approach (Web-based GIS/Mobile Devices)*



Departments

1019 New Members

1019 Classifieds

1021 Member Champions

1022 Certification List

1024 Who's Who in ASPRS

1025 Sustaining Members

1027 Instructions for Authors

1078 Forthcoming Articles

1088 Calendar

1103 Advertiser Index

1103 Professional Directory

1104 Membership Application

PE&RS

October 2012

Volume 78, Number 10

PHOTOGRAMMETRIC ENGINEERING & REMOTE SENSING
The official journal for imaging and geospatial information science and technology

JOURNAL STAFF

Publisher

James R. Plasker
jplasker@asprs.org

Editor

Russell G. Congalton
russ.congalton@unh.edu

Executive Editor

Kimberly A. Tilley
kimt@asprs.org

Technical Editor

Michael S. Renslow
renslow76@comcast.net

Assistant Editor

Jie Shan
jshan@ecn.purdue.edu

Assistant Director – Publications

Rae Kelley
rkelley@asprs.org

Publications Production Assistant

Matthew Austin
maustin@asprs.org

Manuscript Coordinator

Jeanie Congalton
jcongalton@asprs.org

Circulation Manager

Sokhan Hing
sokhanh@asprs.org

Advertising Sales Representative

The Townsend Group, Inc.
asprs@townsend-group.com

CONTRIBUTING EDITORS

Grids & Datums Column

Clifford J. Mugnier
cjmce@isu.edu

Book Reviews

John Iames
liames.john@epamail.epa.gov

Mapping Matters Column

Qassim Abdullah
Mapping_Matters@asprs.org

Website

webmaster@asprs.org



Immediate electronic access to all peer-reviewed articles in this issue is available to ASPRS members at www.asprs.org. Just log in to the ASPRS web site with your membership ID and password and download the articles you need.

Peer-Reviewed Articles

1029 A Supervised and Fuzzy-based Approach to Determine Optimal Multi-resolution Image Segmentation Parameters

Hengjian Tong, Travis Maxwell, Yun Zhang, and Vivek Dey

A novel technique to effectively determine optimal image segmentation parameters for eCognition and improve the segmentation efficiency and accuracy.

1045 Automated Georegistration of High-Resolution Satellite Imagery using a RPC Model with Airborne Lidar Information

Jaehong Oh, Changno Lee, Yangdam Eo, and James Bethel

A new method for automated georegistration of high-resolution satellite imagery using a RPC model with existing airborne lidar data.

1057 Generation of a U.S. National Urban Land-Use Product

James A. Falcone and Collin G. Homer

A proposed method and examples for building a national urban land-use grid representing thematically-detailed classes.

1069 A Flexible Mathematical Method for Camera Calibration in Digital Aerial Photogrammetry

Rongfu Tang, Dieter Fritsch, Michael Cramer, and Werner Schneider

A new family of rigorous and flexible self-calibration additional parameters (APs) and strategies for assessing the full potential of in-situ camera calibration.

1079 Mapping Individual Tree Species in an Urban Forest Using Airborne Lidar Data and Hyperspectral Imagery

Caiyun Zhang and Fang Qiu

A neural network based classifier to identify individual tree species by integrating lidar data and hyperspectral imagery.

1089 Operational Utilization of Aerial Multispectral Remote Sensing during Oil Spill Response: Lessons Learned During the Deepwater Horizon (MC-252) Spill

Jan Svejkovsky, William Lehr, Judd Muskat, George Graettinger, and Joseph Mullin

Oil slick spatial extent and thickness estimation maps derived from a multispectral visible, near-IR and thermal IR aerial imaging system were successfully utilized for multiple applications during the Deepwater Horizon oil spill.

PHOTOGRAMMETRIC ENGINEERING & REMOTE SENSING is the official journal of the American Society for Photogrammetry and Remote Sensing. It is devoted to the exchange of ideas and information about the applications of photogrammetry, remote sensing, and geographic information systems.

The technical activities of the Society are conducted through the following Technical Divisions: Geographic Information Systems, Photogrammetric Applications, Primary Data Acquisition, Professional Practice, and Remote Sensing Applications. Additional information on the functioning of the Technical Divisions and the Society can be found in the Yearbook issue of *PE&RS*.

Correspondence relating to all business and editorial matters pertaining to this and other Society publications should be directed to the American Society for Photogrammetry and Remote Sensing, 5410 Grosvenor Lane, Suite 210, Bethesda, Maryland 20814-2144, including inquiries, memberships, subscriptions, changes in address, manuscripts for publication, advertising, back issues, and publications. The telephone number of the Society Headquarters is 301-493-0290; the fax number is 301-493-0208; email address is asprs@asprs.org.

PE&RS. *PE&RS* (ISSN0099-1112) is published monthly by the American Society for Photogrammetry and Remote Sensing, 5410 Grosvenor Lane, Suite 210, Bethesda, Maryland 20814-2144. Periodicals postage paid at Bethesda, Maryland and at additional mailing offices.

SUBSCRIPTION. Effective January 1, 2012, the Subscription Rate for non-members per calendar year (companies, libraries) is \$420 (USA); \$436 for **Canada Airmail** (includes **5% for Canada's Goods and Service Tax** (GST#135123065)); \$430 for all other foreign.

POSTMASTER. Send address changes to *PE&RS*, ASPRS Headquarters, 5410 Grosvenor Lane, Suite 210, Bethesda, Maryland 20814-2144. CDN CPM #(40020812)

MEMBERSHIP. Membership is open to any person actively engaged in the practice of photogrammetry, photointerpretation, remote sensing and geographic information systems; or who by means of education or profession is interested in the application or development of these arts and sciences. Membership is for one year, with renewal based on the anniversary date of the month joined. Membership Dues include a 12-month subscription to *PE&RS* valued at \$68. Subscription is part of membership benefits and cannot be deducted from annual dues. Annual dues for Regular members (Active Member) is \$135; for Student members it is \$45 (E-Journal – No hard copy); for Associate Members it is \$90 (see description on application in the back of this Journal). An additional postage surcharge is applied to all International memberships: Add \$40 for **Canada Airmail**, and 5% for **Canada's Goods and Service Tax** (GST #135123065); all other foreign add \$60.00.

COPYRIGHT 2012. Copyright by the American Society for Photogrammetry and Remote Sensing. Reproduction of this issue or any part thereof (except short quotations for use in preparing technical and scientific papers) may be made only after obtaining the specific approval of the Managing Editor. The Society is not responsible for any statements made or opinions expressed in technical papers, advertisements, or other portions of this publication. Printed in the United States of America.

PERMISSION TO PHOTOCOPY. The appearance of the code at the bottom of the first page of an article in this journal indicates the copyright owner's consent that copies of the article may be made for personal or internal use or for the personal or internal use of specific clients. This consent is given on the condition, however, that the copier pay the stated per copy fee of \$3.00 through the Copyright Clearance Center, Inc., 222 Rosewood Drive, Danvers, Massachusetts 01923, for copying beyond that permitted by Sections 107 or 108 of the U.S. Copyright Law. This consent does not extend to other kinds of copying, such as copying for general distribution, for advertising or promotional purposes, for creating new collective works, or for resale.

Is your contact information current?

Contact us at members@asprs.org

or log on to <http://www.asprs.org/Member-Area/>
to update your information.

We value your membership.

Operational Utilization of Aerial Multispectral Remote Sensing during Oil Spill Response: Lessons Learned During the Deepwater Horizon (MC-252) Spill

Jan Svejkovsky, William Lehr, Judd Muskat, George Graettinger, and Joseph Mullin

Abstract

A rapidly deployable aerial multispectral sensor utilizing four channels in the visible-near-IR and one channel in the thermal IR was developed along with processing software to identify oil-on-water and map its spatial extents and thickness distribution patterns. Following validation over natural oil seeps and at Bureau of Safety and Environmental Enforcement's (BSEE's) Ohmsett test tank, the system was utilized operationally on a near-daily basis for three months during the Deepwater Horizon (MC-252) spill in the Gulf of Mexico in summer 2010. Digital, GIS-compatible analyses were produced and disseminated following each flight mission. The analysis products were utilized for a multitude of response activities including daily offshore oil recovery planning, oil trajectory modeling, dispersant application effect documentation, beached oil mapping and documentation of the relative oil amount along the spill's offshore perimeter. The system's prime limitation was its relatively narrow imaging footprint and low sun angle requirement to minimize sunglint, both of which limited the total area that could be imaged each day. This paper discusses the system's various applications as well as limitations that were encountered during its use in the Deepwater Horizon incident.

Introduction

Rapid determination of the spatial extents of an oil slick during and after an at-sea spill is vital for evaluating response needs, and initiating and guiding spill response

Jan Svejkovsky is with Ocean Imaging Corporation, 201 Lomas Santa Fe Dr., Suite 370, Solana Beach, CA 92075 (jan@oceani.com).

William Lehr and George Graettinger are with the National Oceanographic and Atmospheric Administration, 7600 Sand Point Way NE, Seattle, WA 98115.

Judd Muskat is with the California Department of Fish & Game, Office of Spill Prevention and Response, 1700 "K" Street, Sacramento, CA 95811.

Joseph Mullin is with Joseph Mullin Consulting, LLC, 8003 Chestnut Grove Road, Frederick, MD 21701. (Retired from Bureau of Ocean Energy Management, Regulation, and Enforcement after this research was conducted).

activities. Just as importantly, oil thickness distributions are beneficial for proper choice of response methods and spatial allocation of response resources. However, accurate oil film thickness/volume estimation remains a difficult challenge (Lehr, 2010; Brown *et al.*, 2005).

The major remote sensing technique for oil spills is visual observations and recordings by a trained observer. Various formulas have been built to link slick appearance with spill thickness. The earliest reported system in the literature was a 1930 report to the US Congress that listed six thickness categories from 0.04 μm to 2 μm . A more widely circulated standard, done by American Petroleum Institute in 1963, closely followed this earlier report. Hornstein (1972) developed a standard that was based upon actual experiments; under controlled laboratory lighting, he spilled known quantities of different crude and refined oils into dishes, then documented their appearances. This standard is still widely used in response guidebooks. It divides oil thickness into five groups ranging from 0.15 μm to 3.0 μm . The European response community has produced its own set of standards, the most widely disseminated being those connected with the Bonn Agreement (Bonn Agreement, 2007). The Bonn Agreement Aerial Surveillance Handbook (BAASH) uses an appearance code based upon previously published scientific papers, small-scale laboratory experiments, mesoscale outdoor experiments and field trials. The visual, appearance-based methodology suffers from three main complications, however. First, any verbal, graphic, or oblique photographic documentation is usually based only on approximate geo-location information obtained through the aircraft's Global Positioning System (GPS). Even if it is later reformatted as input into a computerized Geographical Information System (GIS), the data can contain a great degree of positional error. Second, visual estimation of oil film thickness distribution is highly subjective and, if not done by specially trained and experienced personnel, tends to be inaccurate. Most often the observers' tendency is to overestimate the amount of oil present, resulting in the recovery crews' losing valuable time

Photogrammetric Engineering & Remote Sensing
Vol. 78, No. 10, October 2012, pp. 1089–1102.

0099-1112/12/7810-1089/\$3.00/0

© 2012 American Society for Photogrammetry
and Remote Sensing

“chasing sheens” rather than concentrating on the thicker accumulations. Third, comprehensive visual assessments are impossible at night.

Aerial and satellite imaging can, in principle, provide a convenient means to detect and precisely map marine oil spills, and provide timely information for guiding recovery operations. Advances in imaging technologies within the last two decades have increased the utilization of aerial imaging in oil spill detection and response, and side-looking airborne radar (SLAR) and ultraviolet/infrared (UV/IR) detectors are being used operationally in Europe (Zielinski, 2003; Trieschmann *et al.*, 2003; Brown and Fingas, 2005). Europe’s oil pollution recognition programs are nationally or multi-nationally funded with a fleet of dedicated aircraft equipped with specialized oil-sensing instruments (Bonn Agreement, 2007). No such program of similar magnitude presently exists in the United States. In most cases, observer aircraft are provided by the responsible party, US Coast Guard or a regional/state spill response agency.

On 20 April 2010 the Deepwater Horizon (DWH) oil rig exploded in the Gulf of Mexico and continued to spill oil into the sea until 15 July, 2010 when the wellhead was finally capped. Although the total amount of oil spilled remains under investigation, the spill is widely regarded as the second largest in history, exceeded only by the Mina al Ahmadi spill during the first Gulf War in 1991 (NOAA, 2011). Due to the size of the spill, traditional visual aerial surveys could not provide complete coverage of the spill area on a daily basis. As part of the response, multiple remote sensing technologies and sensors were mobilized. The most frequently utilized data during the response were provided by Synthetic Aperture Radar (SAR) sensors aboard Canadian Radarsat satellites, Moderate Resolution Imaging Spectroradiometer (MODIS) instruments aboard National Aeronautics and Space Administration’s (NASA’s) Aqua and Terra satellites, aerial Side-Looking Airborne Radars (SLARS) flown by Transport Canada and Icelandic Coast Guard, and multispectral visible and thermal infrared imagery flown by USA’s Ocean Imaging Corporation (OI). (Several other imagers, both federal and corporate, collected data primarily for research, test, or baseline documentation purposes but were not deployed on a routine, daily basis and did not provide the imagery for daily response activities.) The volume of remote sensing data collected from these sources and their daily application during the lengthy spill represents to-date the most intense utilization of remote sensing technologies during an oil spill incident. It was also the first instance when maps of oil spill distribution and thickness derived from aerial multispectral visible-near-IR and thermal IR imagery were operationally produced and widely disseminated during various facets of the response effort. This paper focuses on the utilization of the acquired aerial multispectral imaging for the different response activities, how this imaging technology was integrated with the other remote sensing resources, and the major lessons learned from applying the aerial remote sensing technology in such a large-magnitude event.

Background and Methodology

The detection of oil spills has been demonstrated with both aerial and satellite-based instruments. Numerous technology review articles have been published that discuss the various remote sensing approaches and their limitations (e.g., Fingas and Brown, 1997; Brekke and Solberg, 2005; Jha *et al.*, 2008; Lehr, 2010; Fingas and Brown, 2011). For the purposes of this paper the following paragraphs briefly summarize the most commonly recognized instruments with emphasis on their practical, operational application.

The most commonly utilized satellite and aerial sensors are SARs, which detect oil by its surface slick signature. The presence of a surfactant film on the water surface suppresses capillary waves and thus reduces the backscatter return intensity over the slick area. The effect can also be observed with passive instruments such as MODIS when the satellite imagery contains sunglint off the ocean surface (Hu *et al.*, 2009). Present SAR technology is not readily able to distinguish between true oil signatures and biogenic slicks or low-wind affects, however, and is thus sometime subject to a high incidence of false targets. SAR imaging is also not able to quantify oil thickness, rendering even the thinnest (and unrecoverable) sheens the same or very similar as thick oil and oil-emulsion accumulations whose locations are of prime interest for efficient spill response. On the other hand, both satellite and aerial SARs can provide relatively wide spatial coverage, making them very useful (as was the case in the DWH spill) for assessing the total extents of surface oil and their changes in time during a large spill. Additionally, the unique ability of these instruments to penetrate cloud cover and be effective at night allows them to provide updated information with consistent frequency.

Another instrument type that has been tested for oil slick detection and some thickness measurement is the laser fluorosensor. The instrument uses a downward-looking laser to excite fluorescence in floating oil molecules, and detects the fluorescence-caused backradiation in the ultraviolet UV part of the spectrum. Since the instrument is dependent on the excitation effects of its laser, however, the aircraft carrying it must fly very close to the ocean surface (maximum altitude is usually 150 to 180 meters, up to 600 meters for high-powered XeCl excimer laser systems). The result is a thin line of data corresponding to the laser’s track along the aircraft’s flight path. A recently developed scanning laser fluorosensor extends the line of measurements into an “image” path up to 200 meters wide (Brown and Fingas, 2003). The high cost and one-of-a-kind nature of that instrument greatly restricts its operational use. Although laser fluorometry is quite effective at detecting oil on the ocean, the need for extensive criss-cross flying to map even a medium-size spill as well as the obvious possible dangers of flying at such a low altitude under adverse wind conditions limit its operational use. Additionally, under real-world conditions, the Raman signal used for thickness determination with laser fluorometry tends to disappear over films thicker than approximately 10 μm (Lennon *et al.*, 2006), with the signal’s suppression limiting detection and thickness estimation to films in the range of 0.1 μm to 10 μm (Hengstermann and Reuter, 1990; Goodman and Brown, 2005). To our knowledge, laser fluorometry has not yet been successfully utilized for operational support during an actual oil spill.

UV-sensing imagers detect petroleum’s high reflectance in the UV band. This effect occurs even over very thin oil sheens, and UV sensors are thus useful for oil detection and surveillance purposes. As with SAR imaging, however, (although due to different physical properties) the technology provides almost no information on oil thickness, making it of limited use for actual oil spill response where it is important to distinguish the locations of thicker oil accumulations from the usually much larger sheen areas.

As was already mentioned, thermal imaging has shown promise in oil spill mapping. A number of past studies have shown that thermal IR sensors have the potential to identify the thicker oil films (Byfield, 1998) and can be used to direct skimmers to thicker portions of the slick (Fingas and Brown, 1997). One IR-based system utilizing a neural network approach to classify oil slick thicknesses into a number of thickness classes claimed to reach accuracies

of 76 to 82 percent for oil films up to several millimeters thick when a range of sea state and atmospheric parameters were known (Davies *et al.*, 1999). A thermal imager also makes it possible to continue mapping and monitoring the oil spill during nighttime. As previous studies and OI's own research have shown, however, an oil spill mapping effort based solely on IR imagery can be quite complex: oil sheens generally cannot be identified, but thin films may appear cooler than the surrounding water during both day and night, due at least in part to petroleum substances' lower than water emissivity properties. Thicker (and hence darker) crude oil films tend to trap and re-emit solar heat input and thus appear warmer than water during the day. After sundown they revert to appearing cooler due to the emissivity difference.

Visual assessment of oil-on-water thickness is based on optical properties within the visible wavelength range that change with increasing oil thickness. The utilization of a multispectral imaging system configured to maximize the same optical properties can thus represent a potentially more effective extension of the traditional visual oil spill surveys. The visible wavelength range can be further augmented by cameras that image in the near-IR and thermal IR. The vast recent advancements in vis-near-IR multispectral and thermal IR camera technologies provide such systems with significant potential for becoming useful operational tools during oil spill response efforts. With emphasis on developing an easy-to-deploy, operationally useful oil spill mapping system, OI has conducted research since 2004 on oil identification and thickness classification algorithms using a multispectral system in the visible-near-IR-thermal IR wavelength range. The objective was to apply the same general principles of the existing visual oil classification parameters, augmented by near-IR and thermal-IR bands, to drive software that objectively classifies the image pixels into oil thickness classes based on their individual spectral characteristics. In addition to outputting a high resolution, accurately located GIS-compatible map of the oil features, the system should reduce the subjectivity inherent in visual observations made by multiple observers on different days. The emphasis was on operational-oriented image acquisition and processing using portable, relatively inexpensive acquisition and processing hardware that could be quickly mounted in an aircraft-of-opportunity, operated by minimal personnel and produce quantitative map products in near-real-time. For these reasons, a multispectral (a few channels) rather than a hyperspectral (a dozen to 100+ channels) system was used. However, advances in both hyperspectral data cube processing techniques (Boggs and Gomez, 2001), and imaging hardware may render hyperspectral technology practical in such future real-time or near-real-time oil spill mapping systems.

Oil Mapping Algorithm Principles

Previously published research utilizing multispectral imagery for oil thickness determination generally used one of two approaches: multispectral classification where the resulting classes were calibrated for thickness using some external or *in-situ* data (Chouquet *et al.*, 1993; Rogne *et al.*, 1993; Lennon *et al.*, 2006), or the computation of ratios between specific wavelengths and relating the ratio values to oil thickness through laboratory testing (Alhina *et al.*, 1993; Byfield, 1998). Unfortunately, simultaneous field measurements are usually difficult to obtain during a real oil spill. Additionally, the researchers tended to ignore variability due to background water color and illumination (most studies do not even mention whether the aerial and field data were gathered under sunny or cloudy conditions), and their results tend to be very specific for each particular experiment.

This makes the previous studies of little use in applying them to the development of a real-world, operational system.

OI's initial algorithm development was guided by results of experiments in which nadir-viewing reflectance spectra of known thickness films from several crude oils and Intermediate Fuel Oils (IFOs) were obtained while floating on sea water that was sufficiently deep to eliminate bottom reflectance. The initial data were collected only under sunny conditions with sun angles between 25° and 60°. Representative spectra for Alaska North Slope Crude are shown in Figure 1. The reflectances are the result of three primary contributions: reflectance from the oil film itself, upwelling irradiance of the underlying water column, and the oil's fluorescence. Several general observations relevant to the derivation of crude oil thicknesses from multispectral imagery should be noted from these data:

1. No unique reflectance/absorbance peak was found in the visible-near-IR range which independently changes with varying oil thickness. Additionally, the thinner film oil spectra are significantly attenuated by the underlying water reflectance characteristics.
2. For un-weathered oils, the near-IR range contains very little thickness-related information since the reflectances of both, oil films and background water are very low in that part of the spectrum.
3. The greatest thickness-related change in the oil spectra occur within the 570 nm (green) to 675 nm (red) part of the visible spectrum. Some useful thickness-dependant trends also occur in the UV to 470 nm region.
4. For films over deep water (i.e., no bottom reflectance), very little spectral change was measured with films thicker than approximately 0.15 to 0.2 mm for crudes and IFOs, indicating this is the upper thickness detection limit of an algorithm solely based on UV-Vis-Near-IR wavelengths.

It must be noted that the above observations encompass only the wavelength range of approximately 400 nm to 950 nm, which is the typical span of imaging systems using silicon-based Charge-coupled Devices (CCDs) for image capture. This technology does not allow observations in the deep near-infrared. Some specialized instruments such as NASA's Airborne Visible/Infrared Imaging Spectrometer (AVIRIS) have imaging capabilities at longer wavelengths, and Clark *et al.* (2010) developed methodologies using multiple channels in the 1.2 μm to 2.3 μm range in an attempt to quantify the oil/water ratio and thickness of oil emulsions in AVIRIS imagery collected during the DWH spill.

Following the initial algorithm development, OI conducted further experiments over natural oil seeps in the Santa Barbara Channel, California and at Ohmsett - The National Oil Spill Response Research and Renewable Energy Test Facility, located in Leonardo, New Jersey. OI utilized the Digital Multispectral Camera (DMSC-MkII) imager manufactured by SpecTerra Ltd. in Australia. This frame-grabber type imager uses four lenses and four $1,024 \times 1,024$ pixels silicon-based CCDs to yield four data channels with 12-bit radiometric resolution. Each channel's wavelength range is customized with 10 nm-wide interference filters (see Table 1 for further specifications).

In the Ohmsett experiments, the imager was mounted approximately 10 m above the tank's water surface from a "crow's nest" tower on a movable bridge across the tank. Increasingly greater quantities of oil were poured onto the water surface within a set of floating containment squares and dispersed to cover each square (surface breeze prevented the oil film thickness to remain completely homogeneous in each square). Because the tank's depth is approximately 2.5 m and its bottom is painted white, the water column's back-reflectance does not represent conditions normally encountered at sea. To better approximate

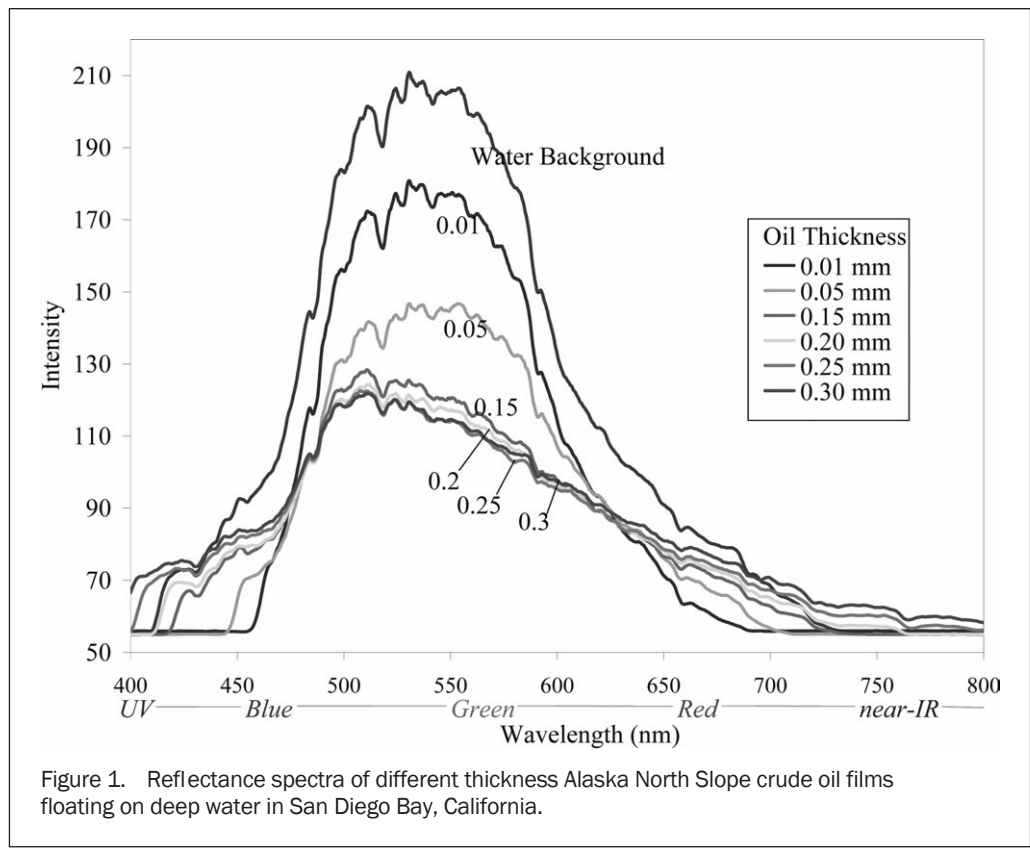


Figure 1. Reflectance spectra of different thickness Alaska North Slope crude oil films floating on deep water in San Diego Bay, California.

TABLE 1. SPECIFICATIONS FOR OI'S SPEC TERRA DMSC M ULTRASPECTRAL IMAGER AND JENOPTIK THERMAL CAMERA

	DMSC Mk-II	Jenoptik IR-TCM640
Detector Type	Progressive-scan CCD	Uncooled Microbolometer
Number of Channels	4 customizable w/10 nm interference filters	1
Image Format	1024 × 1024 pixels	640 × 480 pixels
Spectral Range	400 – 950 nm	7.5 – 14 μm
Dynamic Range	12-bit	16-bit
Thermal Resolution		<70mK
Field of View	29.3° × 29.3°	30° × 23°
Dimensions	25.4 cm × 25.4 cm × 27 cm	153 cm × 91 cm × 111 cm
Weight	16.3kg	1.05kg

background deep-water color and reflectance, a dull canvas tarp painted blue-green was used to cover the bottom of the tank below and around the containment squares. The squares were then imaged as the bridge moved over them (Svejkovsky and Muskat, 2009).

Work over the Santa Barbara Channel oil seeps involved mounting the imaging equipment in aircraft and coordinating simultaneous imaging of suitable oil targets with sampling of the oil's thickness at specific locations from a small vessel. The oil film thicknesses were field-measured using a tank-validated procedure with a clean Plexiglas plate that was dipped through the oil film, retrieved, the adhered oil volume determined, and thickness computed based on the volume and total plate surface area to which the oil adhered (Svejkovsky and Muskat, 2006).

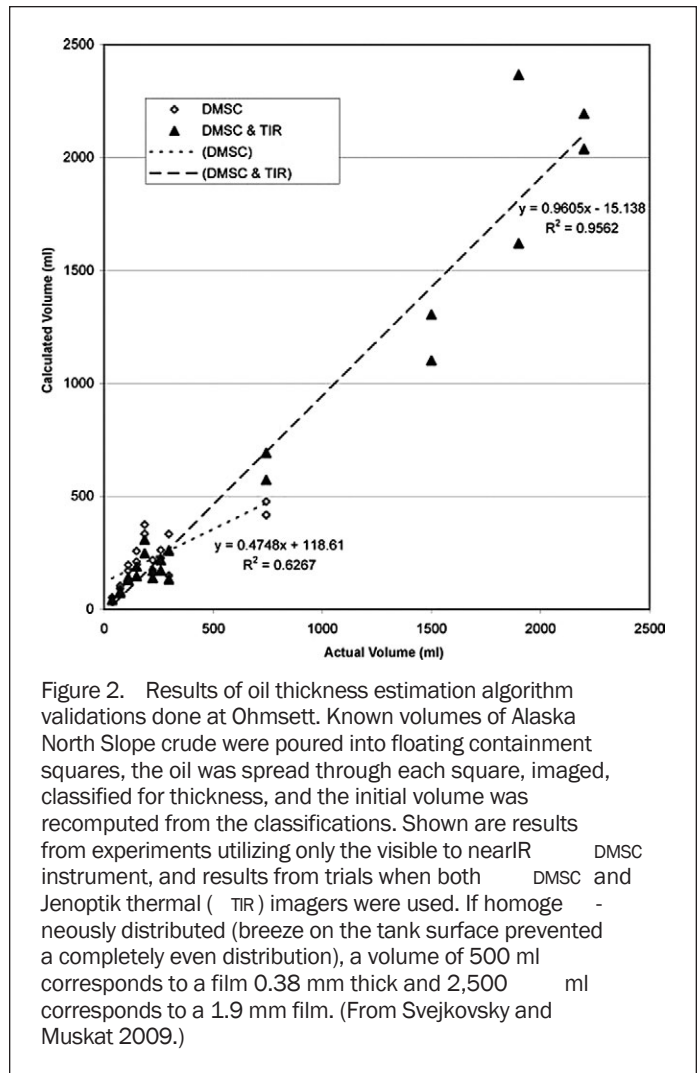
Through experimentation, OI chose 450, 551, 600, and 710 nm to represent a highly efficient channel combination for maximizing the spectral reflectance changes with increasing oil film thickness. The developed oil mapping algorithm is described in more detail in Svejkovsky *et al.* (2008) and Svejkovsky and Muskat (2009). It consists of two steps: The

first step utilizes a neural network classification algorithm applied to the four available DMSC channels to identify all imaged ocean surface areas that likely contain some oil, and to eliminate artifacts caused by sun glint (the most common), high suspended sediment, floating kelp, and seaweeds, etc. The second algorithm, specifically targeting thickness distributions, is then applied only to the pixels believed to contain oil. For each oil-contaminated pixel, it utilizes the deviation of the different available band ratios from the "clear water ratios" (computed in neighboring areas with no oil contamination). The objective is to utilize the ratio deviations from site and time-specific background reflectance (rather than absolute ratio values as was done in previously published studies) to better account for regional differences in water color and illumination characteristics. The thickness-determining algorithm utilizes a fuzzy ratio-based classification to assign each pixel into a thickness range based on the multiple ratios. The actual thickness classes are assigned based on data from experimentally or field-derived look-up tables stored in the algorithm. Most commonly four to six thickness classes can be derived up to the 0.15+ mm upper

thickness determination limits. The algorithm was validated in the field off Santa Barbara and at Ohmsett (Svejkovsky and Muskat, 2009).

OI conducted additional research to add a thermal IR camera to the multispectral system in an effort to both increase thickness determination efficiency and to extend the upper thickness measurement range to more than approximately 0.15 mm. OI used a Jenoptik IR-TCM-640 camera which provides internally calibrated 640 pixel \times 480 pixel images with 16-bit dynamic range and 0.07°C thermal resolution at 7.5 μ m to 14 μ m (see Table 1 for further specifications). Ohmsett experiments were conducted during the summer under both clear and cloudy skies and various sun angles (with surface water and air temperatures ranging 26°C to 27°C and 21°C to 28°C, respectively), and winter under similarly varying sky conditions (with water and air temperatures ranging 2.4°C to 4.5°C and 3.5°C to 5.5°C, respectively). The tests determined that the approximate daytime lower oil detection limit for IR imaging is in the range of 0.01 to 0.02 mm (i.e., thinner oil films are indistinguishable from the surrounding water temperature). This determination agreed with previously published estimates (Hurford, 1989; Belore, 1982). It also implied that significant overlaps exist between the minimal crude oil thickness detection possible with IR imagers and the maximum thickness determination limit of visible wavelength range systems. In OI's experiments, the aforementioned flip in the oil's thermal signature from cooler to warmer than surrounding water occurred within the overlap range (in agreement with previously published reviews such as Fingas and Brown (1997), and the relationship between increasing thickness and increasing apparent temperature appears linear (the maximum routinely tested thickness of fresh oil at Ohmsett was 2 mm). This allows utilization of the multispectral visible wavelength overlap data to "calibrate" the IR band for thickness. As was already noted, changes in reflectance properties within the visible to near-IR spectrum allow thickness-related differentiations to be made with the multispectral sensor up to around the 0.15 mm range, after which the color of the oil films no longer changes appreciably. In the thermal imagery sheens and very thin films are not readily differentiated, but thicker films exhibit distinguishable thickness-related thermal emittance trends, well past the differentiation limits of the visible-near-IR multispectral imager. Figure 2 shows algorithm validation results from Ohmsett experiments in which known volumes of Alaska North Slope crude oil were poured into the containment squares, the oil was spread out in each square and allowed to form patterns of different thicknesses. The squares were then imaged, classified for oil thickness and the total oil volume in each square was calculated from the classification. The results underscore the utility of combining the multispectral visible-near-IR imagery with thermal-IR imagery to achieve better overall accuracy as well as extend the thickness measurement range.

OI's (daytime) thermal IR imaging tests showed a consistent increase in apparent temperatures in increasingly thicker oil films up to the tested 2 mm. The relationship was observed during summer and winter conditions and under both clear and cloudy skies (the slope of the thermal oil-water contrast versus thickness varied with solar input conditions but could be compensated by an offset determined from the visible to near infrared channel overlap range). This is in contrast to Brown *et al.* (1998) who reported no correlation between oil film thickness and thermal signal strength. They based their conclusion on comparisons of thickness measurements within tank-contained slicks made with a subsurface acoustic probe, and relative contrast differences between oil and surrounding



water recorded with an un-calibrated, 8-bit downward-looking analogue thermal camera/VHS tape system. Since the camera yielded only relative brightness and had automatic gain control, it is not known what thermal range each video frame represented (which also contained various solid objects in addition to the water and oil), and hence the thermal increment represented by each greyscale. It is possible that any thermal trend was masked within the 25 to 38 greyscale range of the data (10 to 15 percent range of highest grey level) by frame-to-frame variability in the thermal resolution of the 8-bit images. Perhaps more importantly, however, the vast majority of the measurements were over oil slick portions thicker than 2 mm (and up to 8 mm), i.e., outside the range of our own Ohmsett tests. It is possible that under given solar input conditions the increase in heat emission becomes asymptotic for films exceeding several millimeters. We intend to conduct further research on this subject.

The developed multi-sensor system and processing algorithms were first utilized operationally in California during a crude oil spill from Platform "A" in the Santa Barbara Channel in December, 2008, and an IFO spill during ship-to-ship bunkering operations in San Francisco Bay in October 2009. The total volume of oil spilled in the two incidents is still under investigation, however, all estimates indicate that the Santa Barbara Channel spill (the larger of the two) totaled at most a few thousand liters of crude,

affected a few square kilometers of ocean surface, and direct recovery and associated response operations could terminate after a few days.

Methodology Adaptations for the Deepwater Horizon

Spill Response

Under direction from the National Oceanographic and Atmospheric Administration (NOAA) and British Petroleum (BP), OI was mobilized to aid the DWH Spill response on 01 May 2010. Following equipment installation on-board a NOAA Twin Otter aircraft, the oil mapping system was first utilized on 04 May 2010. In the following days, until 26 July 2010, the OI imaging and NOAA aircraft teams flew one to two imaging missions almost daily, based out of Mobile, Alabama. The imaging equipment consisted of the DMSC MKII multispectral sensor configured with a 450, 551, 600, and 710 nm filter combination, and a Jenoptik IR-TCM640 thermal IR camera system. Both imagers were integrated with an Oxford Technologies 2502 DGPS/IMU positioner with 100 MHz update rate and 2 m circular positioning error under Space Based Augmentation System (SBAS) conditions. OI's custom software was used to auto-georeference and mosaic the acquired image frames. Previous tests with this system configuration and software showed RMS positioning error after the auto-mosaicking of <6 m at 3,040 m flight altitude (Svejkovsky and Muskat, 2009). Most offshore oil mapping missions were conducted at 3,800 m altitude, resulting in 2 m data resolution for the DMSC and 4 m resolution for the Jenoptik IR imagery. Beached and shore-entrained oil mapping missions were conducted at approximately 1,700 m, yielding approximately 0.7 m and 1.5 m spatial data resolutions, respectively.

As was already mentioned, the oil mapping system was previously used operationally on two spills in California. In both cases, the imaging required merely one to five flight lines of a few kilometers in length to completely image the spill-affected area. At 2 m resolution, the DMSC imaging swath is 2,048 m and some overlap is required between adjacent image lines for proper multi-line mosaicking. Already on 04 May 2010 the size of the DWH spill precluded any attempts to map the complete spill area. Since sunglint severely degraded image usefulness of visible wavelength imagery from the DMSC sensor, imaging was limited to several hours in the morning after sunrise and several hours in the afternoon before sunset when low sun angles prevailed. (The thermal IR imagery is not affected by sunglint and could be used throughout the day and night.) These spatial and temporal limitations dictated that the OI team received guidance on which specific target areas within the spill area to image each day. Initially, such guidance and target area prioritization was received independently from the multiple Incident Command Posts (ICPs) that were established. Later in the spill, the Houma, Louisiana ICP became the lead center for guiding the various remote sensing missions.

Another methodological problem that was immediately recognized during the spill was the need for very fast and broad distribution of the image-derived analyses. The prime reasons for this were (a) the immediate need for any oil thickness and location information to help guide on-water recovery operations, trajectory models, etc., and (b) to provide access to the data and analyses for the geographically very dispersed response community. The immediate analysis generation need was hampered by data processing difficulties due to the extreme haze, sun angle and (on some flights) overhead cloud-caused illumination imbalances which affected the visible wavelength image quality. Flight

takeoff timing (often at first light), length, and other logistics also prevented the collection of adequate pre-flight and in-flight calibration data that are normally used for standard application of the above-described oil thickness classification algorithm. These factors contributed to the need for additional, manual processing procedures to maintain quality control and flight-to-flight oil map product consistency. On the other hand, OI's discussions with the various end-user groups made it clear that most of the image-derived product end-users did not have an immediate need for products with highly detailed oil thickness classifications. Instead, the specific need was to quickly obtain GIS-compatible maps of recoverable oil (i.e., relatively thick or emulsified) versus unrecoverable (i.e., sheen). For this reason, the OI team developed a "Rapid Turn-around" class of analysis products that highlighted all imaged oil features thicker than approximately 0.1 mm as a single class. These analyses could be consistently derived much faster from the imagery data and were usually generated in-flight while flying back to the aircraft base in Mobile, Alabama. They were then disseminated as e-mail attachments to a recipient list immediately upon landing.

Following each flight, the acquired data were then reprocessed for multiple oil thickness classes, although the unavailability of calibration data and the sometimes extreme humidity/haze conditions resulted in most data sets to be confidently classified into only four or less thickness range classes. These "Rapid Turn-around" and fully classified products were then made directly available to the situation desk and operations unit at the Houma ICP and to the broader response community through the Environmental Response Management Application[®] (ERMA[®]) web mapping application established by NOAA early in the response. Sample Rapid Turn-around and Full Classification products of the oil spill source area are shown in Plate 1.

ERMA[®] is a web-based mapping application that was designated as the US Government's Common Operating Picture (COP) providing real-time situational awareness to the Government and partner agencies across the response. Data from multiple sources were loaded daily or multiple times a day into a common framework. ERMA[®] provided response and baseline data in this common web-based visualization tool. OI and other remote sensing data products were made available for USCG Command briefings at the Unified Area Command (UAC) and at the ICPs as well as to the National Incident Command (NIC) in Washington, D.C. The incorporation of these data resources supported real-time decision making at all levels of the response as well as for the injury assessment and the subsequent restoration planning that are currently ongoing. ERMA[®] was jointly developed by NOAA and the University of New Hampshire.

Results and Lessons Learned

The OI system was found to be effective in mapping areas of fresh and slightly weathered oil, oil emulsions, and beached or land-entrained oil in various stages of weathering. Plate 2 shows an area containing recently upwelled, unemulsified oil near the Spill Source site, as imaged by OI's multispectral visible-near-IR and thermal IR systems on 06 May 2010. The region generally contained areas of thick, fresh oil which appeared dark brown to the human eye and yellow when rendered with the DMSC's 450, 551, 600 nm for the blue, green, and red components, respectively. In concurrence with OI's previous experimental observations, sheens tended to exhibit elevated reflectances (from surrounding water) in the 450 and 551 nm bands, while thick oil films exhibited suppressed reflectance in the 450 nm, and elevated reflectances in the longer wavelength bands, particularly the

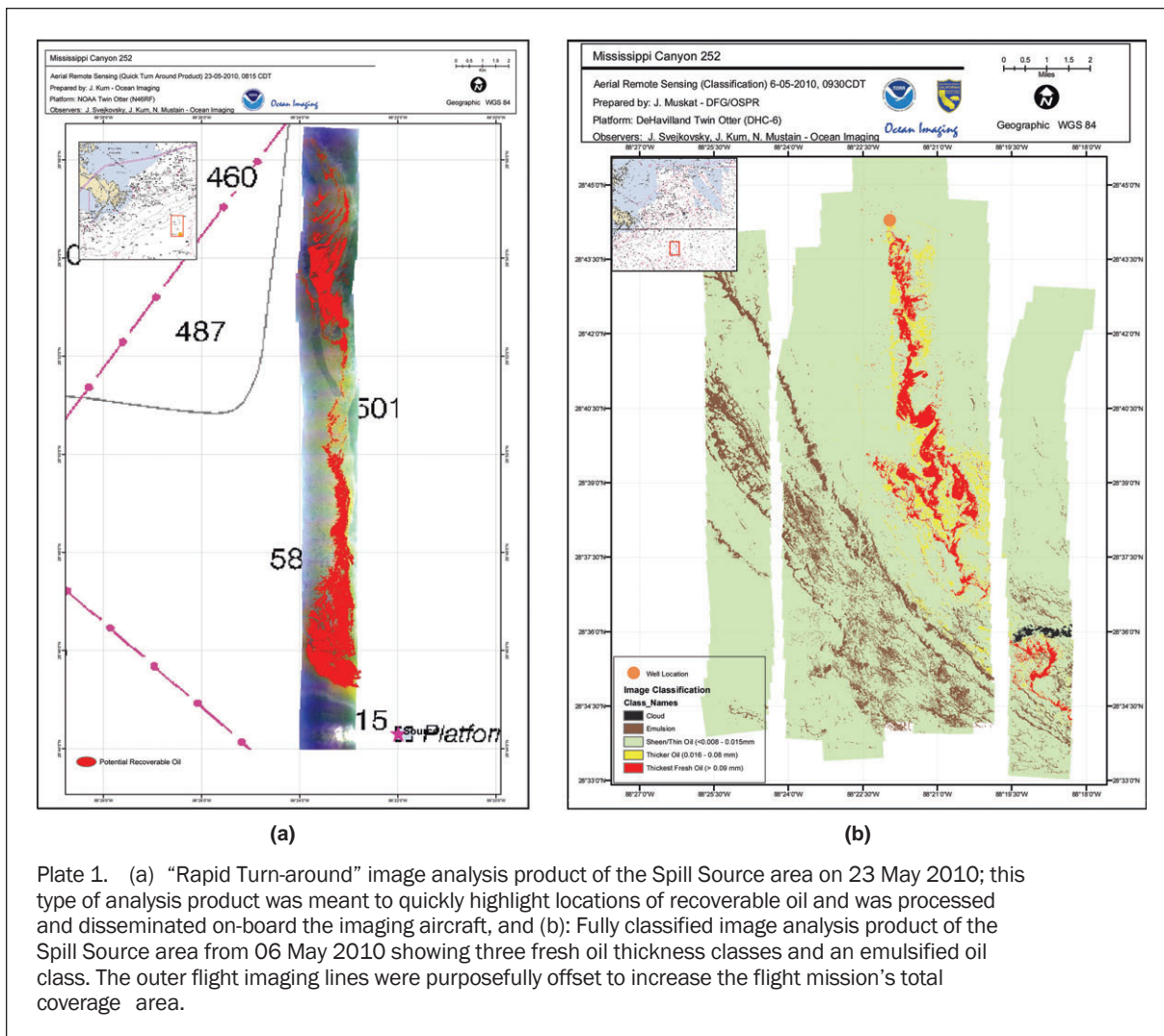


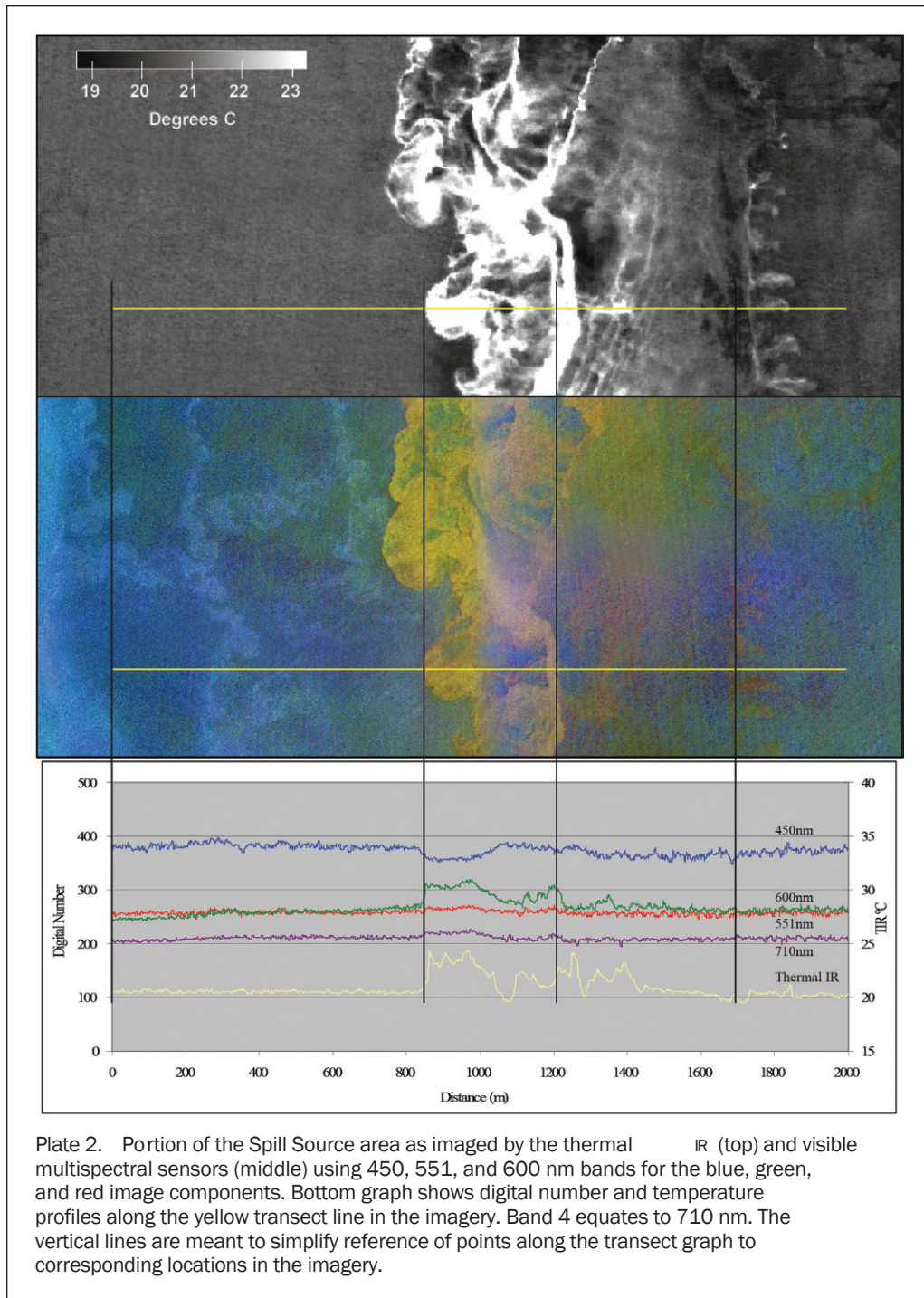
Plate 1. (a) “Rapid Turn-around” image analysis product of the Spill Source area on 23 May 2010; this type of analysis product was meant to quickly highlight locations of recoverable oil and was processed and disseminated on-board the imaging aircraft, and (b): Fully classified image analysis product of the Spill Source area from 06 May 2010 showing three fresh oil thickness classes and an emulsified oil class. The outer flight imaging lines were purposefully offset to increase the flight mission’s total coverage area.

551 nm channel. Early in the response, the thick oil exhibited an IR signature up to several degrees Celsius warmer than the surrounding water. Thinner oil, approximately 0.01 to 0.04 mm thick, as estimated by OI’s Ohmsett experiments and others’ previously published work, appeared cooler by at most a few tenths of a degree Celsius. Very thin oil films, less than approximately 0.01 mm based on previous experimental results, could not be distinguished from the water background in the multispectral visible bands. Very thin sheens were difficult to distinguish from clear water even in the multispectral data, partly due to heavy atmospheric haze that negatively affected the multispectral bands, but also because in many cases, they likely covered essentially the entire ocean surface not covered by thicker oil; hence there were no true “clear water” pixels from which to differentiate the signal levels.

As OI also found to be the case in the previously imaged spills in California waters, the thermal imagery can be relatively easily utilized for rapidly mapping oil features thick enough to be recoverable with the available boom and skimmer resources. The thermal oil signature of freshly upwelled oil near the Spill Source was, however, found to be affected by sea state, since rough seas apparently caused the thick oil to both disperse faster into

thinner films and also to become periodically submerged and lose its heat content. Another factor that we believe caused variability in the thermal signature of the freshly upwelled oil is the application of subsurface dispersants at the point of release on the seafloor. The data shown in Plate 2 were obtained before sustained subsurface dispersant injections began, and thus show thermal and multi-spectral signatures void of any dispersant effects. Later in the spill, the thick fresh oil areas near the Source Site tended to have a less distinct and more uneven heat signature in the thermal data, and often appeared to be more submerged to the naked eye. We postulate this could be due to the effects of the injected dispersants on the oil mixture that did make it to the surface.

OI’s oil thickness classification algorithm was developed for fresh or only mildly weathered oil films. No attempts were thus made to estimate the thickness of oil emulsions, other than to identify them as such in a single “emulsion” class. For the purposes of the image-based oil maps, emulsions were defined as being highly reflective in the near-IR 710 nm band (versus thick fresh crude oil which has only slightly elevated reflectance (Figure 1 and Plate 2)). To the naked eye, emulsions appeared most commonly as bright, orange-red-hued features. Sometimes areas of very dark, likely heavily weathered tar-like oil also appeared within



the bright emulsion features. Plate 3 shows representative multispectral and thermal IR data of an offshore area containing emulsions. The presence of emulsions in this and other areas imaged at other times was qualitatively field-verified by communications from response vessel crews operating in the area. Using the DMSC's 450, 551, and 600 nm channels for blue, green and red components, respectively, the thickest emulsions appear dark purple and the thinner accumulations appear bright red. Relative to clear water areas (likely covered by very thin oil sheen), the emulsion features show depressed reflectances in the 450 and 551 nm bands and increased reflectance in the 600 and 710 nm bands. As was already noted, Clark *et al.* (2010)

subsequently developed an emulsion composition and thickness estimation algorithm based on reflectance spectra of laboratory re-mixed emulsions from an initial DWH sample collected in the field. The algorithm relies on deep near-IR wavelengths available on the hyperspectral AVIRIS instrument but not available with imagers utilized by OI during the response.

Previously published literature tends to state that oil emulsions generally cannot be discerned in thermal IR imagery due to their high water content, which tends to eliminate any thermal contrast between the oil film and the surrounding water. The review article of Fingas and Brown (1997) is often cited as a reference, in which the statement is

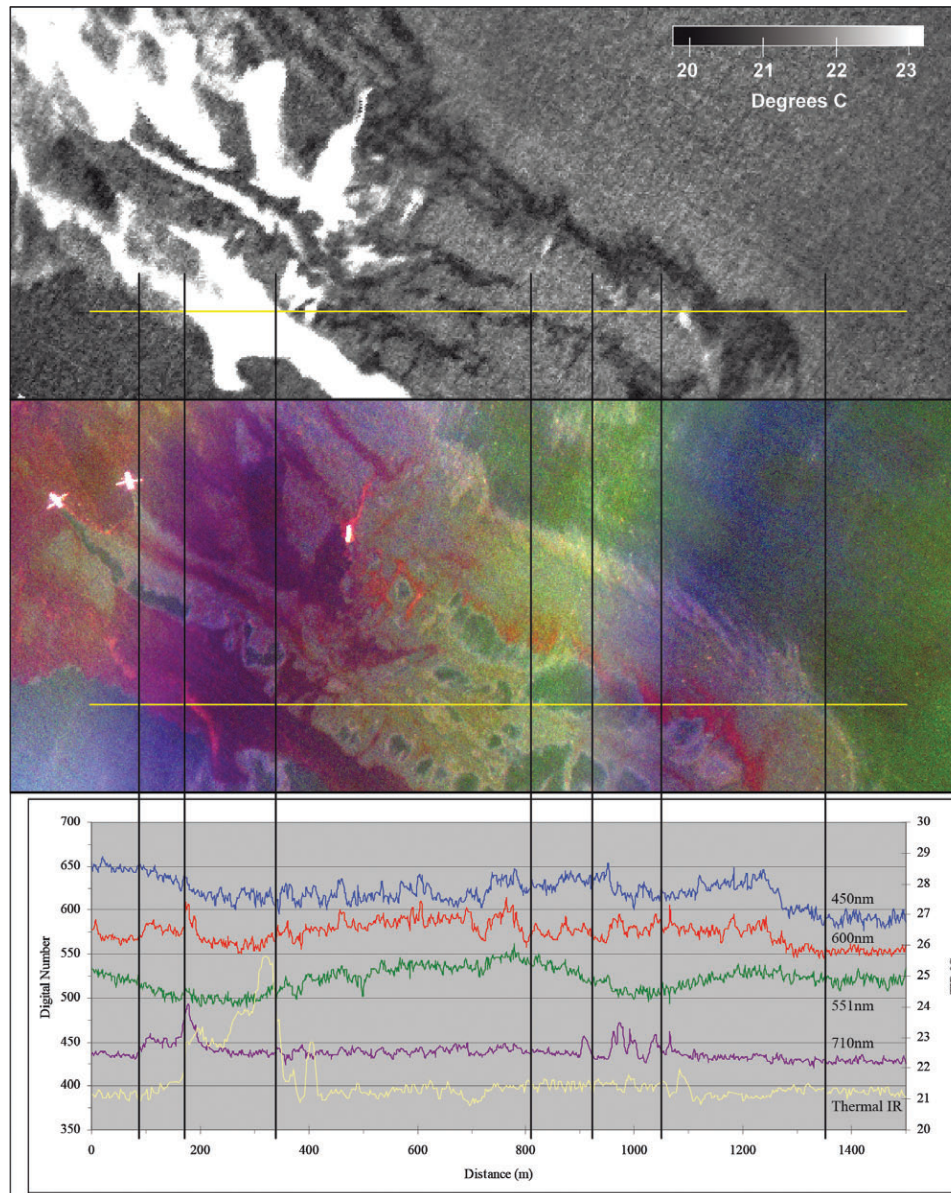


Plate 3. Region containing emulsified oil of different thicknesses and textures, as imaged by the thermal IR (top) and visible multispectral sensors (middle) using 450, 551, and 600 nm bands for the blue, green and red image components. Bottom graph shows digital number and temperature profiles along the yellow line in the imagery. Band 4 equates to 710 nm. The image contains a pair of vessels towing a boom corralling the emulsions for recovery. The vertical lines are meant to simplify reference of points along the transect graph to corresponding locations in the imagery.

linked to work by Bolus (1996). Both, OI's experimental data from Ohmsett with artificially created oil emulsions, and thermal imagery obtained during the DWH spill do not support this contention. At Ohmsett, under partly cloudy and fully overcast conditions and 20°C/16.5 to 19.5°C air/water temperatures, emulsion films containing 20 percent water exhibited thermal signatures similar to pure oil films. Emulsions containing 60 percent water showed a positive thermal contrast compared to water at approximately 0.3 mm and greater thicknesses. In image data containing DWH emulsion features, demonstrated in Plate 3, thin oil emulsions appear slightly cooler than water, similar to thin fresh oil films

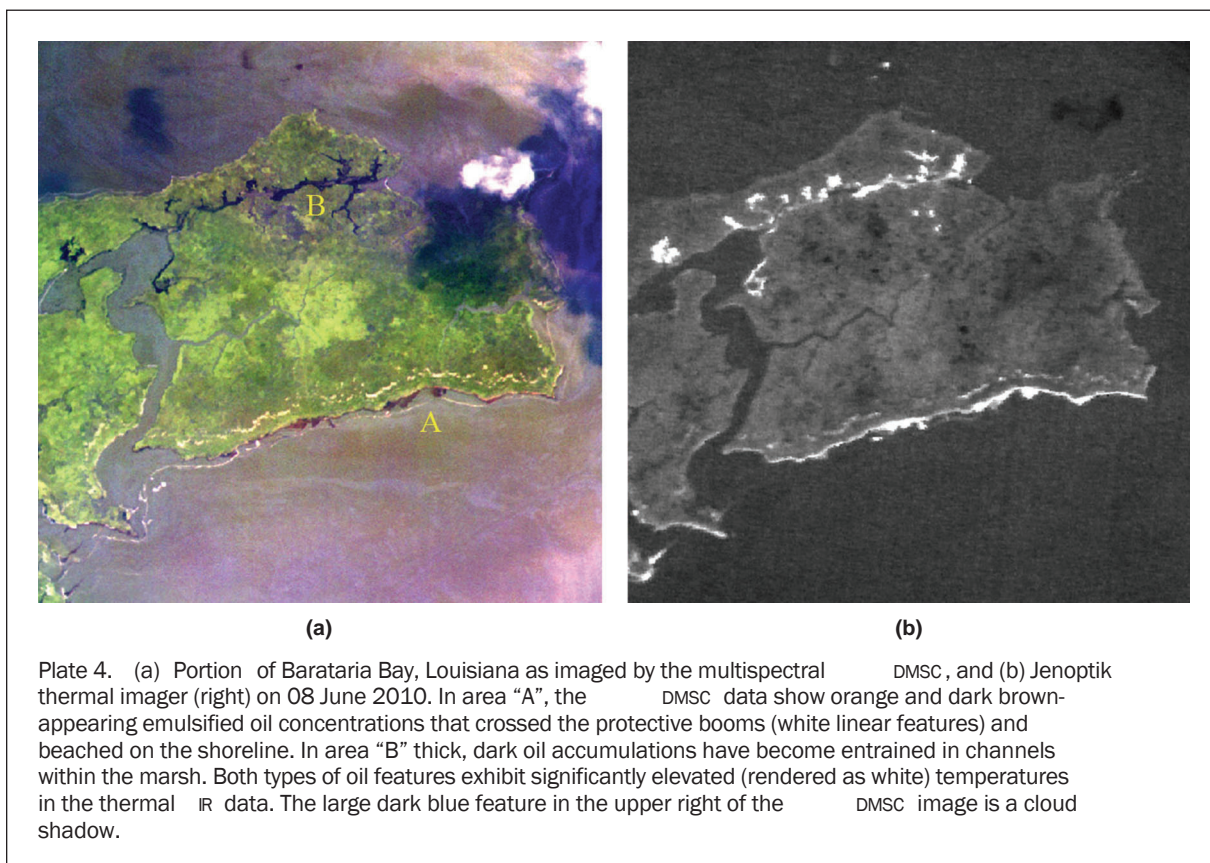
despite their being vastly different in color reflectance. Thick emulsion accumulations appear to trap heat during the day and thus appear much warmer than the surrounding ocean surface. More quantitative analysis of the OI aerial system's imagery with respect to DWH emulsion field samples and ancillary measurements collected during the DWH response by SL Ross Environmental Research Ltd. (Belore *et al.*, 2011) are presently on-going. They also support the premise that floating oil emulsions within a relatively wide range of thicknesses and oil/water ratios can be detected (and some quantitative information extracted) by a modern thermal imager in the 7.5 μm to 14 μm spectral range.

OI's aerial system was also tasked on multiple occasions to scout various shoreline regions for beached oil, and map oil accumulations which have become entrained within the marsh channels of the Mississippi Delta. The oil distribution classifications were then relayed to each region's Shoreline Cleanup Assessment Technology (SCAT) teams either directly or through the ERMA[®] site and were then utilized to help guide the next-day's field operations. Some of the heaviest shoreline and inter-marsh oiling occurred in and around Barateria Bay, Louisiana. Plate 4 shows representative multispectral visible and thermal data from that region. The mapping of oil features along the shoreline and within the marshes required higher spatial resolution imagery than the offshore oil mapping, because the beached accumulations were often elongated along the beach and thus much narrower than the commonly wider, more spread-out offshore oil targets. OI hence conducted its imaging at lower flight altitudes, corresponding to spatial resolutions of 0.7 m and 1.5 m for the DMSC and Jenoptik cameras, respectively. Obviously, such resolutions still compromised the detection of the smaller oil accumulations, but were deemed a reasonable compromise between the need for high spatial resolution and useful daily spatial coverage acquired within the acceptable flight time and sun angle limits.

As can be seen from the data shown in Plate 4, beached or entrained accumulations of orange-colored emulsions and thick, dark weathered oil could be readily detected in the multispectral data as well as in the thermal imagery where such accumulations usually appeared warmer than the surrounding land and water by several degrees Celsius. Unlike in the offshore areas, however, the added complexities of vegetation and land features with highly variable visible/near-IR light reflectance and thermal IR emission

characteristics produced many more potential false targets. For example, heavy beached accumulations of dark organic matter such as dead eel grass had visible and near-IR reflectance characteristics very similar to the dark, thick oil accumulations in both the DMSC data and the naked eye. The thermal IR often provided differentiation capabilities, since the weed accumulations tended to have much lower heat emission characteristics than was typical for dark, weathered oil. Such considerations precluded the application of any automatic oil-detection algorithm without significant manual editing by the OI image analysts. In a number of instances after the earliest shoreline/marsh mapping missions, OI worked interactively with some of the SCAT teams by providing them with coordinates of uncertain oil-like targets and having the SCAT personnel report back on the true identity of the targets after their field work the following day. This greatly aided in "fine tuning" the image classification procedure to better eliminate potential false targets specific to the Mississippi Delta environment in future data sets. It should be noted that the available combination of visible, near-IR and thermal IR wavelengths proved much more effective in accurately mapping oil in the marsh areas than would have been possible with only the visible/near-IR or thermal IR imagery alone.

The unprecedented and novel daily availability of the aerial multispectral imagery and oil thickness/weathering state classification products initially met with skepticism in some cases, but also faced the formidable obstacle of initially not having established protocols for their utilization within the various response groups and activities. However, the response groups in multiple command centers and in the field soon began to formulate strategies to take advantage of the new type of information. As awareness of the OI analyses grew, so too did the demand for including multiple



target areas in each day's mission. The following applications exemplify diverse successful utilizations of the OI aerial system:

Determination of Regional Oil Volume and Trajectory

The aerial imagery acquired over the Spill Source site was commonly utilized to establish the daily pattern and relative quantity of oil emanating to the surface. With limited imaging time, the multiple flight line image acquisitions were adjusted on-site to match the direction of the heaviest oil distribution and document the pattern and trajectory direction of the main oil slick. One such analysis is shown in Plate 1b. (As the Plate 1b sample demonstrates, the imaging swaths were sometimes purposely offset to increase the overall spatial coverage of the Spill Source imaging missions.) The multispectral/IR imagery and thickness classification products were further augmented by OI's capture of carefully framed oblique images (using digital SLR cameras) and written observer reports (which helped to extend the "information horizon" beyond the immediate limits of the image and classification data sets). These three combined elements were especially helpful to the Houston ICP where they heightened situational awareness and contributed significantly to the safe conduct of simultaneous operations (SIMOPS) in the source area. In particular, the multispectral imagery and thickness classes were integrated with surface SIMOPS charts by the survey support team in Houston and these, together with the obliques and observer reports, were transmitted to the offshore captains to aid them in visualization of the relative positions of the many surface vessels and the upwelling oil.

The data were also utilized by NOAA's oil distribution modeling team to supplement information from visual observations produced by the NOAA trained observers flying from several forward locations along the coast.

Satellite SAR and airborne SLAR imagery were used extensively to track the spatial extents of the DWH spill. In mid-May the imagery began to show an extension of the overall slick expanding southward into the Gulf of Mexico, raising fears that the oil will be entrained in the Gulf of Mexico Loop Current and thus be transported eastward to ecologically sensitive areas such as the Florida Keys. Because SAR imagery does not provide information on the state or thickness of the oil causing the low-backscatter signature, the SAR data could not by itself be used to evaluate the magnitude of the inherent threat. NOAA (and other response groups) thus directed the OI system to document the state of oiling along the southern periphery of the SAR-derived oil slick boundary.

The magnitude of the oil spill extent prevented the OI team from contiguously mapping the entire area. Instead, with visual observation showing that the vast majority of the southernmost SAR-sensed oil slick feature is due only to very light sheen, imaging was done only over features representing thicker oil. All the features corresponded to relatively light emulsion accumulations. The detailed aerial maps allowed the evaluation of the relative amount of oil nearing the Loop Current boundary. The combination of large-scale SAR or SLAR-derived imagery and aerial multispectral/IR imaging was utilized several more times during the DWH spill response, each time with multispectral imagery being used to determine the state or type of oiling within a feature of interest initially revealed by the SAR data.

A unique use of the imagery was as a check on the effectiveness of subsurface dispersant application. Because the Twin Otter/OI platform maintained a consistent observational record of the surface oil above the source, it provided a history of relative surface volume. Typically, untreated oil

would reach the surface from the leaking riser in a matter of a few hours, while the reduced droplet size of effectively treated oil would slow the rise time indefinitely. By examining the surface slick before and a few hours after commencement of subsurface dispersant use, a qualitative assessment of effectiveness can be made. The imagery and image-derived oil thickness analyses were utilized as part of Environmental Protection Agency-sanctioned evaluation of the subsurface dispersant application concept early in the response.

As was noted above, the Rapid Turn-around analysis products identifying potentially recoverable oil features were produced in-flight by the OI team and disseminated as e-mail attachments immediately upon landing, as well as being loaded into the ERMA[®] COP within hours. By June 2010 the list of recipients also included a number of at-sea vessels taking part in the offshore recovery operations who thus gained rapid access to the aerial image-based information.

Imaging of Aerial Dispersant Applications

Aerial dispersants were heavily utilized throughout the spill response. Plate 5 shows data from an imaging flight coordinated with the dispersant application team. To eliminate the risk of direct contact with personnel, aerial dispersant releases were usually conducted a considerable distance from the Spill Source area which contained the highest concentration of vessels and crew. This resulted in most of the dispersant being released on weathered and emulsified oil. Although there has been debate in the past whether aerial dispersant applications can be effective on oil emulsions, OI's imagery supported the notion that, at least in the DWH spill, Corexit 9500 aerial dispersant application on floating oil emulsions was likely effective under wind and sea-state conditions existing in the imaged region. Plate 5 shows image data from a single flight line that transected a region containing concentrations of emulsified oil (appearing bright orange to the naked eye), and a neighboring region that had been sprayed with dispersant approximately 30 minutes before the image acquisition. Visual observations showed both a color and textural change upon application of the dispersant: the oil substance changed from a bright orange to yellow in appearance, and began to be drawn out into thin striations by the near-surface wind-induced current. The color changes were also recorded in the multispectral imagery, but the most dramatic change was documented by the thermal IR imager. The un-dispersed floating emulsions had a typical, distinct cooler-than-water signature (indicating relatively thin films). This signature was completely lost in areas affected by the dispersant spray, suggesting that the dispersant-affected oil had submerged into the water column which the thermal imager cannot penetrate. The imagery acquired in conjunction with both, aerial and subsurface dispersant applications continues to be used by multiple groups evaluating the effectiveness of dispersants in the DWH incident and the utility of dispersants for future spills.

Mapping of Beached and Land-entrained Oil

One of the most useful aspects of the marsh imaging missions to the field response crews was the imagery's ability to reveal oil accumulations deep within the marsh channels. In many cases such channels were quite difficult and very time consuming to scout by field crews in vessels, and could not readily be reached by foot. The image-derived oil distribution maps could thus be used to direct and thus maximize efficiency of the field SCAT resources.

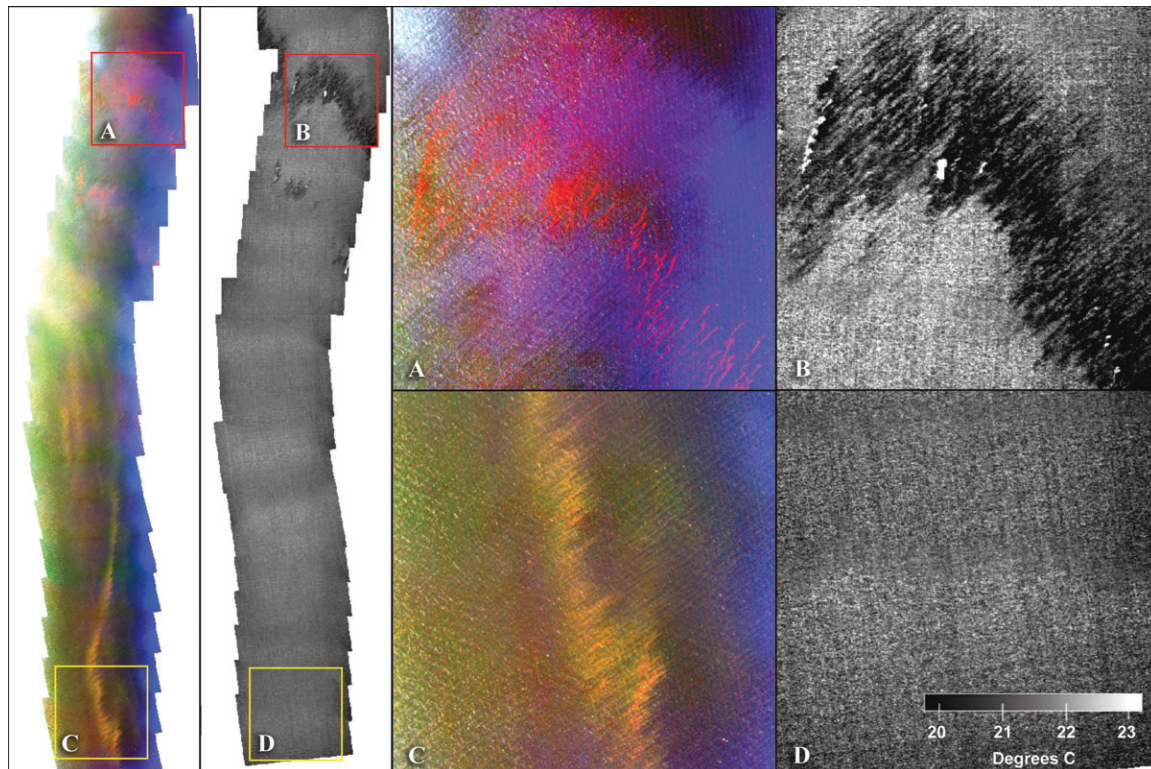


Plate 5. Multispectral color (450, 551, and 600nm) and thermal imagery along a flight line that transected an area with emulsions where no dispersant was applied (top) and a region where dispersant was sprayed over floating oil emulsions approximately 30 minutes before (bottom). At right are enlargements of portions of the flight line showing the un-dispersed oil (A = multispectral, B = thermal), and dispersed oil (C = multispectral, D = thermal). Most of the un-dispersed emulsions exhibit a cooler-than-water thermal signature (thinner), with a few smaller areas appearing warmer (thick). The dispersed oil had likely sunk into the water column and is thus no longer discernible in the thermal data.

Following initial coordinated field validation efforts between the OI imaging team and SCAT teams surveying several island shorelines in Barataria Bay, OI overflights were conducted to guide future SCAT surveys. As mentioned above, OI oil thickness and distribution maps were available to response personnel through the ERMA[®] viewer. Additionally, OI's oil distribution and thickness maps were transmitted directly using email to the SCAT Unit coordinators in KMZ file format for direct viewing in Google Earth[™].

Imaging System Limitations

The greatest recognized shortcoming of the OI aerial imaging system was the limited area that it could image each day, which limited, in turn, the number of response groups or activities that could utilize each day's image analysis products. For example, if the OI system was tasked to image sections of the Mississippi Delta marshes to aid that region's SCAT and Natural Resource Damage Assessment (NRDA) teams, the system could often not be utilized that day for aiding offshore oil recovery operations. In an attempt to take full advantage of the capabilities of the OI system and crew, data collection over specifically requested areas and targets of opportunity was also often conducted on the out-bound and in-bound legs of flight missions primarily intended to image the source or some impacted length of shoreline.

MODIS, SAR, and SLAR imaging platforms provided daily broad, synoptic views of the interpreted slick extents, but

were unable to provide thickness classifications or discriminate between sheen and thicker recoverable oil. Conversely, the OI system was providing daily or twice daily (weather permitting) location-focused, data sets and detailed thickness class analyses, but was limited in geographic scope to a total collection footprint of 350 to 500 km² per flight mission. As a consequence, an attempt was made to bridge the information gap between the two available remote sensing options using available (off-the-shelf) large-format aerial mapping systems that (although unable to provide a synoptic view of the full slick extents like SLAR, or detailed thickness classes like OI) could provide on-demand, multispectral, intermediate-scale, low-latency imagery data over operationally significant marine and/or shoreline areas of up to ~5000 km² per day (daylight and weather permitting). One such system tested was the Leica ADS40 which was optimized and flown by Northrup Grumman to acquire and deliver (within several hours of acquisition) four-band (visible and near-IR) orthoimagery with a ground sample distance of approximately 5 meters (after ~100:1 pixel aggregation).

The test-use of the large-format photogrammetry systems proved to have three prime hindrances for daily, operational use, however: (a) Not being specifically designed for oil spill mapping, there was no postprocessing mechanism to generate oil-specific analysis products from the data. The system operators simply provided raw, unclassified imagery, limiting its use and interpretation to a few specialists; (b) the data files were too large (several hundred MB, even when

compressed at reduced spatial resolution) for practical mass dissemination to the broad response community as e-mail attachments or web-based ERMA[®] downloads; and (c) No thermal IR image component was available which, as is discussed below, proved highly useful for oil thickness characterizations under operational conditions. It should be noted that the test deployments of the large-format photogrammetry systems (as well as non-operational data acquisitions by hyperspectral systems like NASA's AVIRIS) were in most cases initial attempts at their utilization strictly for oil spill mapping, and their utility will likely increase with more research and experience. In the OI system case, oil spills covering 700 to 1,000 km² can be likely fully covered in two missions each day. In spills generating slicks beyond this size extent (as in the case of the DWH incident) only portions of the entire region can be effectively imaged, processed and disseminated as oil characterization analyses.

Collaborative feedback between the OI data acquisition/processing crew, and SCAT and Natural Resource Damage Assessment (NRDA) teams also revealed an important limitation of the use of multispectral/thermal imaging for identifying oiled land areas during the DWH spill. The oil mapping procedures utilized by OI relied on the ground substrate's alteration in visible/near-IR reflectance and thermal IR emittance properties directly caused by the presence of oil. In marsh areas subject to tidal flushing the amount of oil adhering to the substrate after one or more tidal cycles was variable, especially in areas covered with marsh grasses that could be fully, partially, or only intermittently coated with oil residue. While heavily coated grass regions were identified in the imagery with apparently good consistency, lightly coated regions were difficult or impossible to separate from surrounding unaffected marsh. One concept suggested but not attempted during the spill response is to try to identify the oil's presence on flora indirectly through changes in plant stress, as measured by changes through time in indices such as the Normalized Difference Vegetation Index (NDVI) (Rouse *et al.*, 1973). With the voluminous field data collected by the various SCAT and NRDA teams and imagery time series suitable for NDVI change analysis collected by OI as well as several other sources, the concept invites further investigation. Another possibility is the addition of a UV-sensing camera to the system that could potentially reveal hydrocarbon fluorescence on the plant leaves and stems.

Conclusions

Experience gained through the operational application of OI's multispectral oil mapping system during the DWH spill invites a number of main conclusions about the utilization of such aerial remote sensing as part of oil spill response:

- An aerial system combining visible-near-IR multispectral and thermal IR imaging capabilities can provide information useful for a multitude of spill response activities. This assumes, as was the case with the OI system, that instead of providing the response community with raw imagery (potentially subject to misinterpretation) the data are first processed into meaningful analysis products, documented, and disseminated in a timely manner.
- The ability to classify the imaged oil signal into a high-resolution, GIS-compatible map of thickness classes is an important new asset for spill response and complements the use of SAR and SLAR data that do not have thickness quantification capabilities. For most response activities, however, it is sufficient to classify the oil films into just a few thickness categories, primarily separating sheen and very thin oil films from thicker accumulations. Response activities such as skimming, boom-towing, surfactant spraying, *in-situ* burning, and SCAT surveys are governed by actionable oil and are not likely to alter strategies based on

extremely precise knowledge of oil thickness variability. This fact significantly enhances the utility of aerial oil mapping systems under highly variable "real world" conditions that make absolute oil film thickness measurement extremely difficult.

- In addition to their utilization during actual spill response, the aerial image data provide unique, permanent documentation of oil spill patterns and events in spatial resolution generally not possible with visual survey-derived maps and records. This documentation can then be utilized for post-event analysis, injury assessment and research.
- For large spills, the limitations in imaging time due to acceptable sun angles and the cameras' relatively narrow field of view limit the aerial systems' utilization to specific areas or targets of interest, rather than for mapping of the entire spill. Visual aerial surveys done by trained observers likely remain much more time and cost-effective for frequent, rapid overviews of large spill events.
- The aerial imaging and subsequent oil-identification/characterization processing proved useful for both, offshore and shoreline response activities. In the case of mapping oiled vegetation, however, our experience suggests that detection of lightly oiled areas through direct detection of oil residue may be very difficult or impossible with the developed techniques. This capability could be potentially enhanced with the addition of a UV sensor and/or through indirect detection of changes in the plants' chlorophyll vigor.
- The relatively novel availability of the aerial multispectral imaging capabilities and analysis products in the DWH case resulted, especially in the beginning, in the potential underutilization of the information by some response groups and individuals who did not have the mechanism or infrastructure to use the data in their work protocols. As the availability of both satellite and aerial remote sensing becomes more commonplace during oil spill events, it is important to plan for and rehearse the inclusion of this type of information in response activities.

Acknowledgments

The initial spill mapping system development work was funded by research grants from California Department of Fish & Game's Office of Spill Prevention and Response (OSPR) and the Bureau of Ocean Energy Management, Regulation, and Enforcement (formerly the US Minerals Management Service, presently Bureau of Safety and Environmental Enforcement). The operational use of the system during the DWH spill was funded by British Petroleum, with aircraft and pilot crew generously made available to OI by NOAA. We greatly thank BP's Robert M. Frost for his many contributions to this work, both during the response and during preparation of the manuscript.

Disclaimer

The views expressed in this paper are solely those of the authors and do not represent the official views of the US Government, the State of California, or British Petroleum.

References

- Alhinai, K.G., M.A. Khan, A.E. Dabbagh, and T. Bader, 1993. Analysis of Landsat Thematic Mapper data for mapping oil slick concentrations - Arabian Gulf Oil-Spill 1991, *Arabian Journal for Science and Engineering*, 18(2):85-93.
- Belore, R.C., 1982. A device for measuring oil slick thickness, *Spill Technology Newsletter*, 7(2):44-47.
- Belore, R.C., K. Trudel, and J. Morrison, 2011. Weathering, Emulsification, and chemical dispersibility of Mississippi Canyon 252 crude oil: Field and laboratory studies, *Proceedings of the International Oil Spill Conference 2011*, 23-26 May, Portland, Oregon, unpaginated USB flash drive.

- Boggs, T., and R.B. Gomez, 2001. Fast hyperspectral data processing methods, *Proceedings of SPIE*, 4383, pp. 74–78.
- Bolus, R.L., 1996. Airborne testing of a suite of remote sensors for oil spill detecting on water, *Proceedings of the Second Thematic International Airborne Remote Sensing Conference and Exhibition*, 24–27 June, San Francisco, California, III:743–752.
- Bonn Agreement, 2007. *Bonn Agreement Aerial Surveillance Handbook*, Version 25, October 2007, URL: <http://www.bonnagreement.org/eng/doc/2007%20report%20on%20aerial%20surveillance.pdf> (last date accessed: 05 July 2012).
- Brekke, C., and A.H.S. Solberg, 2005. Oil spill detection by satellite remote sensing, *Remote Sensing of Environment*, 95:1–13.
- Brown, C.E., and M.F. Fingas, 2003. Review of the development of laser fluorosensors for oil spill application, *Marine Pollution Bulletin*, 47:477–484.
- Brown, C.E., and M.F. Fingas, 2005. Review of current global oil spill surveillance, monitoring and remote sensing capabilities. *Proceedings of the 28th Arctic and Marine Oil Spill Program (AMOP) Tech. Seminar*, 07–09 June, Calgary, Canada, pp. 789–798.
- C.E. Brown, M.F. Fingas, J-P. Monchalain, C. Neron, and C. Padioleau, 2005. Airborne oil slick thickness measurements: Realization of a dream, *Proceedings of the Eighth International Conference on Remote Sensing for Marine and Coastal Environments*, Ann Arbor, Michigan, 8 p.
- Byfield, V., 1998. *Optical Remote Sensing of Oil in the Marine Environment*, Ph.D. dissertation, University of Southampton, School of Ocean and Earth Science.
- Chouquet, M., R. Hedon, G. Vaudreuil, J-P. Monchalain, C. Padioleau, and R. H. Goodman, 1993. Remote thickness measurement of oil slicks on water by laser ultrasonics, *Proceedings of the 1993 International Oil Spill Conference*, 29 March-01 April 1993, Tampa, Florida, pp. 531–536.
- Clark, R.N., G.A. Swayze, I. Leifer, K.E. Livo, R. Kokaly, T. Hoefen, S. Lundeen, M. Eastwood, R.O. Green, N. Pearson, C. Sarture, I. McCubbin, D. Roberts, E. Bradley, D. Steele, T. Ryan, R. Dominguez, and the Airborne Visible/Infrared Imaging Spectrometer (AVIRIS) Team, 2010. *A Method for Quantitative Mapping of Thick Oil Spills Using Imaging Spectroscopy*, USGS Open-File Report, 2010-1167, 51 p.
- Davies, L., J. Corps, T. Lunel, and K. Dooley, 1999. *Estimation of Oil Thickness*, AEA Technology Report, AEAT-5279(1), 34 p.
- Fingas, M.F., and C.E. Brown, 1997. Review of oil spill remote sensing, *Spill Science & Technology Bulletin*, 4(4):199–208.
- Fingas, M.F., and C.E. Brown, 2011. Oil Spill Remote Sensing: A Review, *Oil Spill Science and Technology: Prevention, Response, and Clean Up* (M. Fingas, editor), Elsevier, Burlington, Massachusetts, pp. 111–169.
- Goodman, R., and C.E. Brown, 2005. Oil detection limits for a number of remote sensing Systems, *Proceedings of the Eighth International Conference on Remote Sensing for Marine and Coastal Environments*, 18–19 May, Altarum Conferences, Halifax, Nova Scotia, 8 p.
- Hengstermann, T., and R. Reuter, 1990. Lidar fluorosensing of mineral oil spills on the sea surface, *Applied Optics*, 29(22):3218–3227.
- Hornstein 1972. *The Appearance and Visibility of Thin Oil Films on Water*, U.S. Environmental Protection Agency, Report EPA-R2-72-039, Cincinnati, Ohio.
- Hu, C., L. Xiaofeng, W.G. Pichel, and F.E. Muller-Karger, 2009. Detection of natural oil slicks in the NW Gulf of Mexico using MODIS imagery, *Geophysical Research Letters*, 36, L01604, doi:10.1029/2008GL036119.
- Hurford, N., 1989. Review of remote sensing technology, *The Remote Sensing of Oil Slicks* (A.E. Lodge, Editor), John Wiley and Sons, Chichester, UK, pp. 7–16.
- Jha, M.N., J. Levy, and Y. Gao, 2008. Advances in remote sensing for oil spill disaster management: State-of-the-art sensors technology for oil spill surveillance, *Sensors*, 8:236–255.
- Lehr, W. 2010. Visual Observation and the Bonn Agreement, *Proceedings of the Thirty-third Arctic and Marine Oilspill Technical Program Technical Seminar*, Environment Canada, Ottawa, Ontario), pp. 669–678.
- Lennon, M., S. Babichenko, N. Thomas, V. Mariette, G. Mercier, and A. Lisin, 2006. Detection and mapping of oil slicks in the sea by combined use of hyperspectral imagery and laser induced fluorescence, *EARSel eProceedings*, 5:1–9.
- NOAA, 2011. URL: <http://response.restoration.noaa.gov/oil-and-chemical-spills> (last date accessed: 05 July 2012).
- Rogne, T., I. Macdonald, A. Smith, M.C. Kennicutt, and C. Giammova, 1993. Multispectral remote sensing and truth data from the Tenyo-Maru oil spill, *Photogrammetric Engineering & Remote Sensing*, 59(3):391–397.
- Rouse, J.W., R.H. Haas, J.A. Schell, and D.W. Deering, 1973. Monitoring vegetation systems in the Great Plains with ERTS, *Proceedings of the Third ERTS Symposium*, NASA SP-351, I:309–317.
- Svejkovsky, J., and J. Muskat, 2006. Real-time detection of oil slick thickness patterns with a portable multispectral sensor, *Final Report for U. S. Minerals Management Service Contract 0105CT39144*, 37 p.
- Svejkovsky, J., J. Muskat, and J. Mullin, 2008. Mapping oil spill thickness with a portable multispectral aerial imager, *Proceedings of the International Oil Spill Conference 2008*, 04–08 May, Savannah, Georgia, unpaginated USB flash drive.
- Svejkovsky, J., and J. Muskat, 2009. Development of a portable multispectral aerial sensor for real-time oil spill thickness mapping in coastal and offshore waters, *Final Report for U. S. Minerals Management Service Contract M07PC13205*, 33 p.
- Trieschmann, O., T. Hunsenger, L. Tufte, and U. Barjenbruch, 2003. Data assimilation of an airborne multiple remote sensor system and of satellite images for the North and Baltic Sea, *Remote Sensing of the Ocean and Sea Ice* (C.R. Boastater, Jr. and R. Santoleri, editors), SPIE, Bellingham, Washington, pp. 51–60.
- Zielinski, O., 2003. Airborne pollution surveillance using multi-sensor Systems, *Sea Technology*, 44:28–32.

(Received 10 August 2011; accepted 13 December 2011; final version 06 February 2012)